Molecular Therapy
Oncolytics
Original Article

Intravenous Injections of a Rationally Selected Oncolytic Herpes Virus as a Potent Virotherapy for Hepatocellular Carcinoma

Yong Luo,[1,4] Chaolong Lin,[1,4] Wenfeng Ren,[1] Fei Ju,[1] Zilong Xu,[1] Huiling Liu,[1] Zeng Yu,[1] Jun Chen,[1] Jun Zhang,[1] Pingguo Liu,[2,3] Chenghao Huang,[1] and Ningshao Xia[1]

[1]State Key Laboratory of Molecular Vaccinology and Molecular Diagnostics, National Institute of Diagnostics and Vaccine Development in Infectious Diseases, School of Public Health, Xiamen University, Xiamen, China; [2]Department of Hepatobiliary Surgery, ZhongShan Hospital Xiamen University, Xiamen, China; [3]Fujian Provincial Key Laboratory and Chronic Liver Disease and Hepatocellular Carcinoma, ZhongShan Hospital Xiamen University, Xiamen, China

As a clinical setting in which novel treatment options are urgently needed, hepatocellular carcinoma (HCC) exhibits intriguing opportunities for oncolytic virotherapy. Here we report the rational generation of a novel herpes simplex virus type 1 (HSV-1)-based oncolytic vector for targeting HCC, named Ld0-GFP, which was derived from oncolytic ICP0-null virus (d0-GFP), had a fusogenic phenotype, and was a novel killer against HCC as well as other types of cancer cells. Compared with d0-GFP, Ld0-GFP exhibited superior cancer cell-killing ability *in vitro* and *in vivo*. Ld0-GFP targets a broad spectrum of HCC cells and can result in significantly enhanced immunogenic tumor cell death. Intratumoral and intravenous injections of Ld0-GFP showed effective antitumor capabilities in multiple tumor models, leading to increased survival. We speculated that more active cell-killing capability of oncolytic virus and enhanced immunogenic cell death may lead to better tumor regression. Additionally, Ld0-GFP had an improved safety profile, showing reduced neurovirulence and systemic toxicity. Ld0-GFP virotherapy could offer a potentially less toxic, more effective option for both local and systemic treatment of HCC. This approach also provides novel insights toward ongoing efforts to develop an optimal oncolytic vector for cancer therapy.

INTRODUCTION

Hepatocellular carcinoma (HCC) is the sixth most common malignancy and the third most common cause of cancer-related death worldwide.[1,2] Although curative treatments such as liver resection, liver transplantation, and local ablation have improved the outcome in early stage HCC, most patients are not considered as candidates for these therapies because of an advanced tumor stage or inadequate liver function at the time of diagnosis.[3] This limits their treatment to fewer options, such as target-oriented chemotherapeutic methods and inhibitor drugs. HCC patients generally present with poor prognosis; no effective treatment is available for most patients, and the 5-year relative survival rate for patients with advanced stage HCC is only below 11%.[4] Therefore, a more innovative and effective treatment for dealing with advanced stage HCC is required to improve patient survival.

In this regard, oncolytic virotherapy offers a promising therapeutic option for treating advanced stage HCC, with tremendous advantages, such as tumor selectivity, safety, effectiveness, immunomodulation, and fewer adverse effects.[5,6] The lead oncolytic virus (OV) in HCC clinical trials, JX-594, has demonstrated evidence of clinical benefit and been granted orphan drug status by the US Food and Drug Administration (FDA).[7] In 2015, OV T-VEC had shown therapeutic benefit against melanoma and become the first FDA-approved oncolytic virotherapy to treat advanced melanoma.[8] To date, a number of OVs, including adenovirus, reovirus, measles, herpes simplex virus, enterovirus, Newcastle disease virus, and vaccinia, have shown single-agent clinical activity and evidence of clinical synergy with immune checkpoint blockade.[9,10]

Among the OVs, human herpes simplex virus 1 (HSV-1) is one of the agents having several features that meet the requirements for oncolytic virotherapy, and various forms of genetically modified vectors have been developed for cancer therapy.[5,11] The most advanced candidates, including T-Vec, G207, 1716, G47Δ, and HF10, have been evaluated in clinical trials, stating evidence of benefits in treating various types of advanced cancer, such as melanoma, glioma, head and neck cancer, and breast cancer.[12,13] Some efforts have been made to test the antitumor activity of HSV-1-based OVs in preclinical models of HCC, with some evidence of antitumor efficacy.[14–19] A

Received 18 July 2019; accepted 22 September 2019;
https://doi.org/10.1016/j.omto.2019.09.004.

[4]These authors contributed equally to this work.

Correspondence: Chenghao Huang, PhD, State Key Laboratory of Molecular Vaccinology and Molecular Diagnostics, National Institute of Diagnostics and Vaccine Development in Infectious Diseases, School of Public Health, Xiamen University, Xiamen, China.
E-mail: huangchenghao@xmu.edu.cn
Correspondence: Pingguo Liu, MD, Department of Hepatobiliary Surgery, ZhongShan Hospital Xiamen University, Xiamen, China.
E-mail: pgliu@xmu.edu.cn

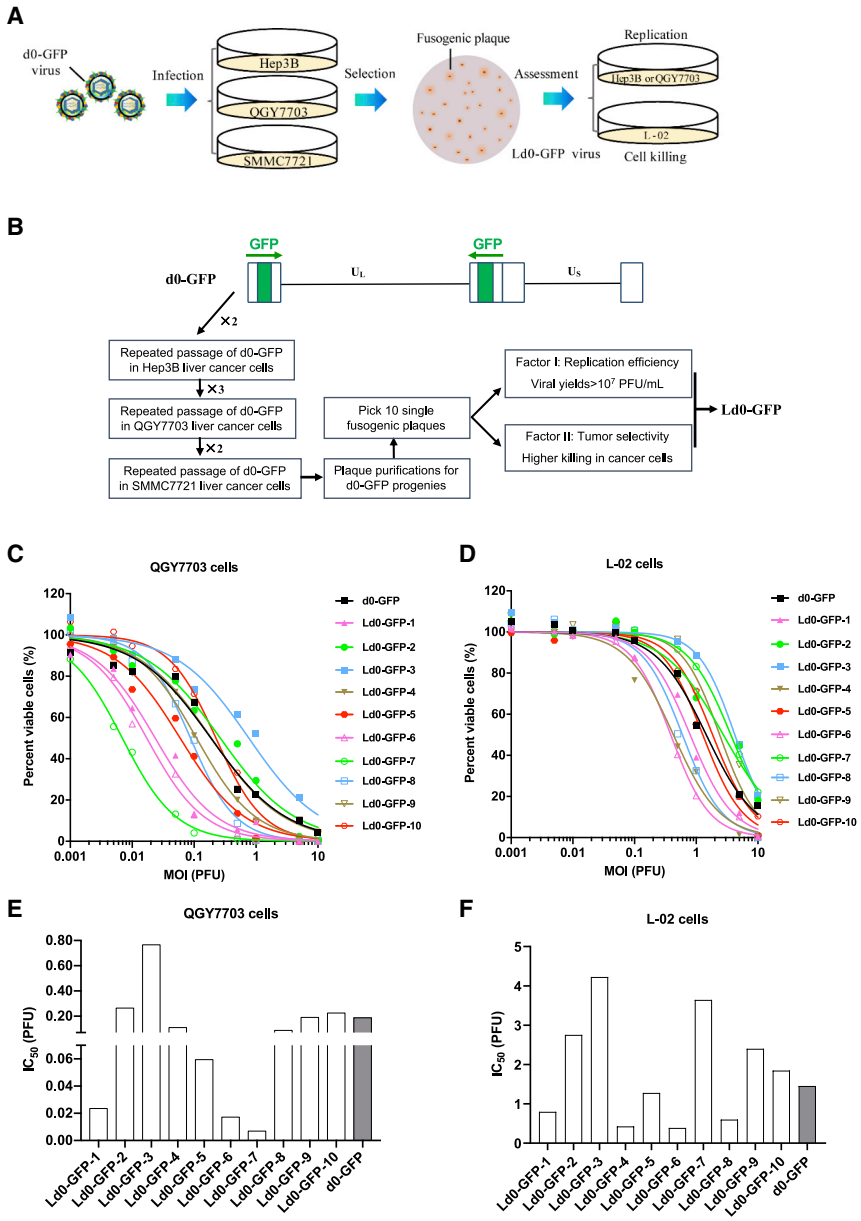

Figure 1. Development of an ICP0 Deletion HSV-1 Virus Targeting HCC

(A) Schematic diagram of developing Ld0-GFP in HCC cell lines, including repeated infection, fusogenic plaque selection, and assessment of viral replication and cell killing. (B) Route map for generating fusogenic d0-GFP progenies and assessing their viral replication efficiency and cell-killing ability. (C) Cell viability was measured in various infected QGY7703 cell lines at 72 h after virus infection. (D) Cell viability was measured in various infected L-02 cell lines at 72 h after virus infection. (E) IC_{50} was calculated in various infected QGY7703 cell lines. (F) IC_{50} was calculated in various infected L-02 cell lines.

number of HSV-1-based oncolytic vectors were designed to target HCC using tissue-specific promoters to drive the expression of an essential viral gene,[20–22] however, few efforts have concentrated on engineering OV cellular specificity and enhancing its antitumor potency against HCC.[23] New approaches to the treatment of HCC are being continuously investigated to facilitate the development of treatments with superior efficacy and lower toxicity.

d0-GFP is an ICP0-null, replication-selective HSV-1 virus, as previously described.[24,25] ICP0-null HSV-1 exploit interferon (IFN)-signaling defects in a number of different tumor types. ICP0 is required to stimulate the translation of viral mRNA in quiescent cells, and it plays a key role in blocking IFN-induced inhibition of viral infection,[25] so ICP0-null HSV-1 replicates more efficiently in cancer cells than in normal cells. Here we introduced a rational design and generated OV Ld0-GFP for targeting HCC, which was selected and obtained by repeated passage of d0-GFP in HCC cells and has superior oncolytic activity and tumor selectivity. Ld0-GFP enhances the oncolytic activity by forming large syncytia, and it induces immunogenic cell death in a variety of HCC cell types. In this study, the oncolytic activity of Ld0-GFP against HCC was investigated both *in vitro* and *in vivo*, and the safety profile of Ld0-GFP was investigated in immunocompetent mice. Such a safe and potent OV seems to be a good choice as a treatment for patients with HCC. These results add value to our understanding of the mechanisms of action of tumor-specific oncolytic vectors.

RESULTS

Development of a Novel OV against HCC

To generate the oncolytic HSV-1 vectors for HCC, we first repeated passage of d0-GFP in Hep3B, QGY7703, and SMMC7721 cell lines, and we screened the fusogenic d0-GFP progenies for targeting HCC (Figure 1A). The screening strategy is depicted in Figure 1B. For every round of d0-GFP passage, the cells were infected with viruses at an MOI of 1 and then harvested at 72 h post-infection for subsequent re-infection. After seven rounds of repeated infection, the d0-GFP progenies, which can form fusogenic plaque, were subjected to single-plaque purification, and those that can form syncytia like plaque were selected for preliminary assessment.

To obtain the most potent OVs for targeting HCC, ten fusogenic d0-GFP progenies were picked out and evaluated by testing their replication difference in U-2 OS cells and cell-killing ability on both HCC cell lines (QGY7703) and the hepatic normal cell line (L-02). OV,

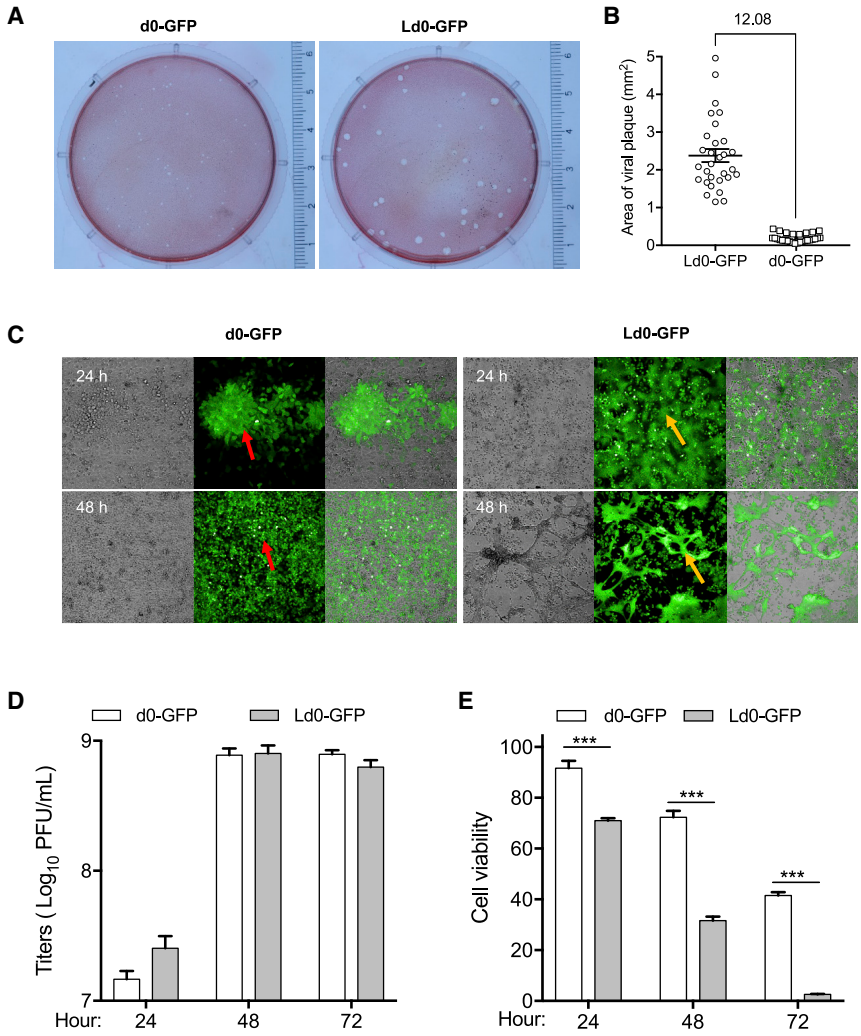

Figure 2. Characteristics of HCC Targeting Oncolytic Virus, Ld0-GFP

(A) Plaque assays of Ld0-GFP and d0-GFP virus on SMMC7721 monolayers. 200 PFU per dish for each virus was used in this assay. (B) 30 random plaques were selected from each virus-infected dish, and the average area of individual plaque was calculated. In addition, the fold change between the average size of Ld0-GFP plaques and d0-GFP plaques is shown. Data are shown as means ± SEM. (C) Viral replication assays were performed on SMMC7721 cells at an MOI of 0.05 PFU/cell. Ld0-GFP and d0-GFP replication patterns were monitored at 24 or 48 h after virus infection. Red arrows indicate virus-infected cells and regular plaques. Orange arrows indicate virus-infected cells and fusogenic plaques. Cells were observed using Operetta High Content Imaging System (PerkinElmer), with a 10× objective. (D) Replication assays were performed on U-2 OS cells at different time points after virus infection. (E) Cell-killing assays were performed on U-2 OS cells at different time points after virus infection. Graphs represent pooled data from three independent experiments. Values are the means of three independent experiments; data are shown as means ± SEM. Data were analyzed by unpaired two-tailed Student's t tests.

which had the greatest replication efficiency and relatively higher tumor-killing selectivity, was selected for further assessment. It showed that d0-GFP-7 had highest replication efficiency among those fusogenic d0-GFP progenies, and it had almost equivalent replication efficiency to d0-GFP (Figure S1). After the comparative evaluation of their cell-killing ability in HCC cell lines (QGY7703) and the hepatic normal cell line (L-02), compared to d0-GFP, we discovered d0-GFP-7 (named Ld0-GFP) with good tumor selectivity, which exhibited high lytic capacity in HCC cells but low lytic capacity in liver normal cells (Figures 1C and 1D). Our data showed that the dose required to kill 50% of cells (IC_{50}) of Ld0-GFP was at least 26-fold lower than that of d0-GFP in QGY7703 cells, but the IC_{50} of Ld0-GFP was at least 2.5-fold higher than that of d0-GFP in L-02 cells (Figures 1E and 1F), suggesting Ld0-GFP was a superior candidate as a selective killer against HCC.

To assess the oncolytic characteristics of Ld0-GFP, we first compared the plaque size between d0-GFP and Ld0-GFP in SMMC7721 cells. The plaque size of Ld0-GFP was significantly larger than that of d0-GFP due to the syncytia-forming ability of Ld0-GFP (Figures 2A and 2B). During the infection, Ld0-GFP could induce SMMC7721 cancer cell fusion so as to exhibit higher cell-killing activity, and the obvious cell death was only observed at 24 h post-infection of Ld0-GFP (Figure 2C). U-2 OS cells are widely accepted as a common cell model for studying HSV-1 replication and yield. After ten rounds of viral propagation in U-2 OS cells at an MOI of 0.005, Ld0-GFP progenies were syncytial and homogeneous (Figure S2).

Next, we evaluated the replication efficiency and oncolytic potency of Ld0-GFP and d0-GFP in U-2 OS cells. As shown in Figures 2D and 2E, Ld0-GFP had better viral yields than d0-GFP only at 24 h post-infection, and later Ld0-GFP and d0-GFP showed similar replication efficiency. However, Ld0-GFP induced significantly higher cell killing than d0-GFP at 24, 48, and 72 h post-infection. Although Ld0-GFP and d0-GFP showed comparable replication efficiency, the oncolytic potency of Ld0-GFP was significantly enhanced in U-2 OS cells, suggesting that the oncolysis-induced cell fusion may contribute to the enhanced cell-killing capability of Ld0-GFP against HCC at late stage.

Ld0-GFP Targets a Broad Spectrum of HCC Cancer Cells with Improved Oncolytic Activity

To explore the oncolytic efficacy of Ld0-GFP *in vitro*, we first compared the cell-killing effects of d0-GFP and Ld0-GFP viruses

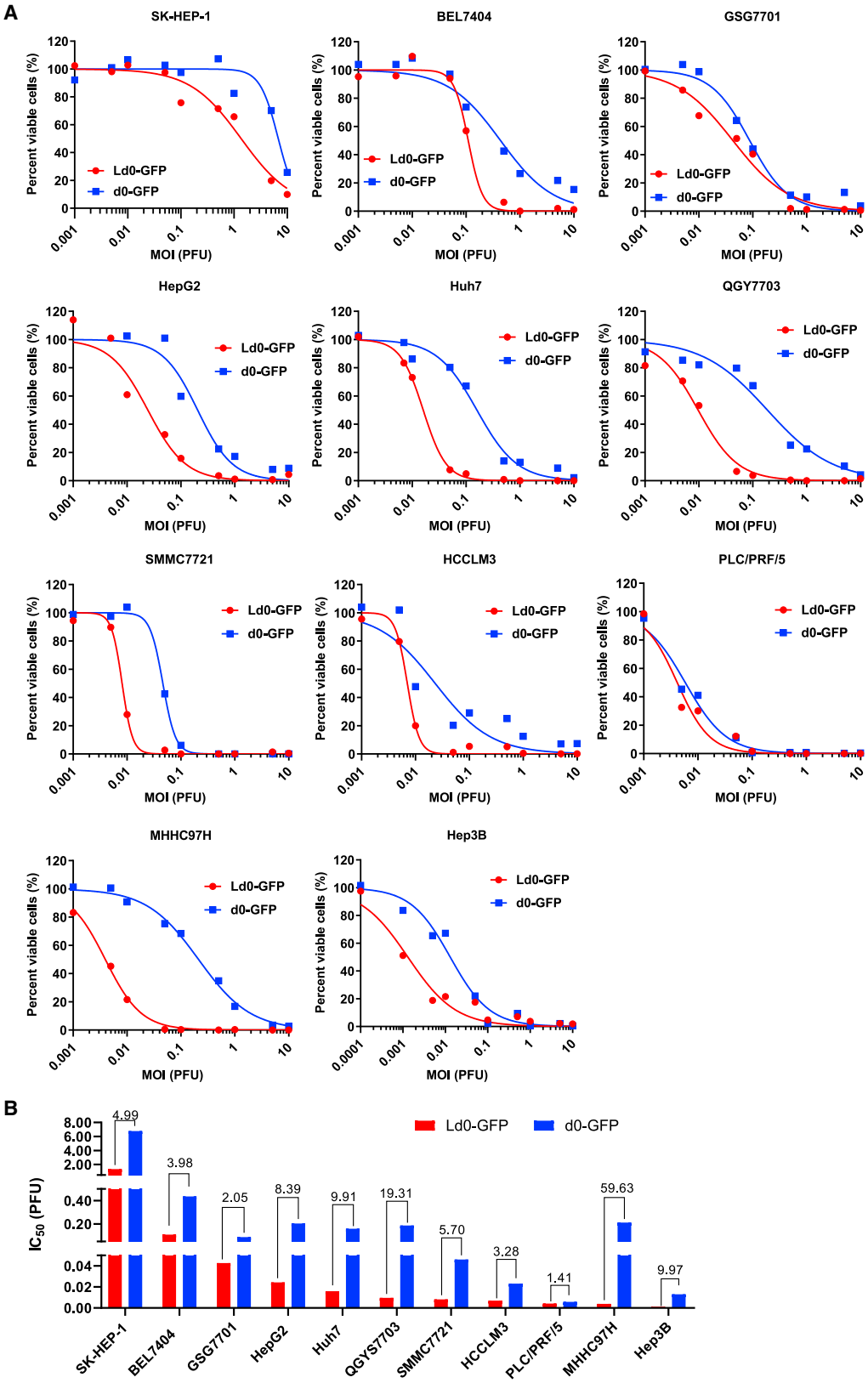

(legend on next page)

on various cultured human HCC cell lines. Of the 11 HCC cell lines that we tested, Ld0-GFP showed markedly enhanced oncolysis compared to d0-GFP (Figure S3; Figure 3A). As shown in Figure 3B, the IC_{50} of Ld0-GFP was at least 5-fold lower than that of d0-GFP in HepG2, Huh7, QGY7703, MHHC97H, and Hep3B cells, and the IC_{50} of Ld0-GFP was at least 2-fold lower than that of d0-GFP in the remaining HCC cell lines, besides PLC/PRF/5 in which the IC_{50} of Ld0-GFP was only 1.41-fold lower than that of d0-GFP. Our data showed Ld0-GFP exhibited increased cell-killing ability not only in high permissive HCC cell lines (HCCLM3, PLC/PRF/5, and Hep3B) but also in less permissive HCC cell lines (SK-HEP-1, BEL7404, and MHHC97H). All these data suggested Ld0-GFP showed superior antitumor capabilities and targets a broad spectrum of HCC cancer cells. Moreover, we tested the *in vitro* activity of the viruses in the mouse H22 cells, and the IC_{50} of Ld0-GFP was at least 2-fold higher than that of d0-GFP irrespective of the relatively low permissivity of mouse cells to HSV-1 (Figure S4). Additionally, our data showed Ld0-GFP exhibited increased cell-killing ability in non-HCC tumor cells, such as H1299 and HCT116 cells (Figures S5A–S5C).

Ld0-GFP Induces Strong Immunogenic Cell Death in HCC Cell Lines

To explore the cell death types involved in Ld0-GFP-induced oncolysis, we examined the apoptosis markers after treatment with Ld0-GFP or d0-GFP. Annexin V/propidium iodide (PI)-labeled fluorescence-activated cell sorting (FACS) analyses showed significant upregulation of annexin V staining at 24 h after viral infection in four HCC cell lines (Figure 4A). Ld0-GFP induced stronger cell apoptosis than d0-GFP in HCC cell lines, and this induction of cell apoptosis was in a dose-related fashion (Figure 4B). However, due to the cell destruction ability of OVs, the cells may be directly destructed when exposed to a high dosage of virus infection, thus the percentage of cell apoptosis was relatively lower in some HCC cells after treatment with OVs at an MOI of 10.

Similar results were obtained when we determined the late apoptosis or necrosis at 24 h after viral infection in four HCC cell lines (Figure S6). To determine the immunogenic profile of virus-infected HCC cell lines, HCC cell lines were infected with Ld0-GFP or d0-GFP at various MOIs. The supernatants harvested from the infected cells were analyzed for expression of the immunogenic cell death (ICD) determinants (extracellular ATP and HMGB1) at 24 h after viral infection. The secreted ATP and HMGB1 were evidently upregulated in the supernatants of Ld0-GFP-infected HCC cells compared to d0-GFP-infected HCC cells, and this induction of secreted ATP and HMGB1 was in a dose-related fashion (Figures 4C and 4D). All these data suggested Ld0-GFP induced stronger immunogenic cell death by activating the ICD pathway compared to d0-GFP.[26]

Safety Profile of Ld0-GFP in BALB/c Mice

To evaluate the safety and potential toxicity of Ld0-GFP, we established two different toxicity evaluation models, including the murine lethal challenge model and systemic challenge model (Figures 5A and 6A). For the murine lethal challenge model, the BALB/c mice were challenged through a single intracerebral inoculation of Ld0-GFP or d0-GFP (1×10^5 plaque-forming units [PFU] per dose). Mice were challenged with HSV-1 wild-type strain KOS (1×10^4 PFU per dose) as a parallel positive control.

It was observed that 90% of mice survived in the Ld0-GFP-challenged group and in the d0-GFP-challenged group compared to the KOS-challenged group, while all mice died in the KOS-challenged group (Figure 5B). The results showed that Ld0-GFP and d0-GFP exhibited comparably reduced neurovirulence *in vivo*. On days 1, 5, 15, and 30, the histological analysis of whole brains of virus-injected mice and vehicle-injected mice was performed by H&E staining. Obvious pathological abnormality was observed in the brains of KOS-injected mice, but not in those of the Ld0-GFP-injected mice and d0-GFP-injected mice (Figure 5C). It was observed that the brain tissue around the KOS-injected site was severely injured compared to that around the Ld0-GFP- or d0-GFP-injected site, which led to the deaths of KOS-injected mice within 1 week. Although slight injury was found around the injection route of brain tissue both in d0-GFP-injected mice and Ld0-GFP-injected mice on day 5 post-injection, all mice finally survived and recovered to normal.

Moreover, we established a systemic challenge model to evaluate the toxicity of Ld0-GFP in mice through a single high dose of intravenous injection of virus (5×10^7 PFU per dose) or PBS (vehicle). A significant difference in body weight between the Ld0-GFP-injected group and the KOS-injected group was observed, and there was no difference in body weight between the Ld0-GFP-injected group and the d0-GFP-injected group during the course of the study (Figure 6B). On days 1, 5, 7, and 30, the histological analysis of vital tissues of virus-injected mice and vehicle-injected mice (n = 2 for each group), including heart, liver, spleen, lung, and kidney, was performed by H&E staining. No obvious pathological abnormality was observed in hearts, livers, spleens, and kidneys of virus-injected mice (Figure 6C). Acute lung injury was observed in KOS-injected mice, but not in Ld0-GFP-injected mice and d0-GFP-injected mice (Figure 6C). All the evidence supports the conclusion that Ld0-GFP is relatively safe in mice.

Preclinical Evaluation of Ld0-GFP in HCC Mouse Models

To further evaluate the antitumor potential of Ld0-GFP *in vivo*, we established three different preclinical tumor models, including the subcutaneous xenograft nude mice model bearing Huh7 and Hep3B HCC (Figure 7A) and the syngeneic HCC mouse model

Figure 3. Oncolytic Effect of Ld0-GFP in HCC Cell Lines

(A) Cell viability assays were performed on a panel of HCC cell lines at 72 h after Ld0-GFP or d0-GFP infection (MOI = 0.001–10 PFU/cell), respectively. (B) IC_{50} was calculated in various infected HCC cell lines.

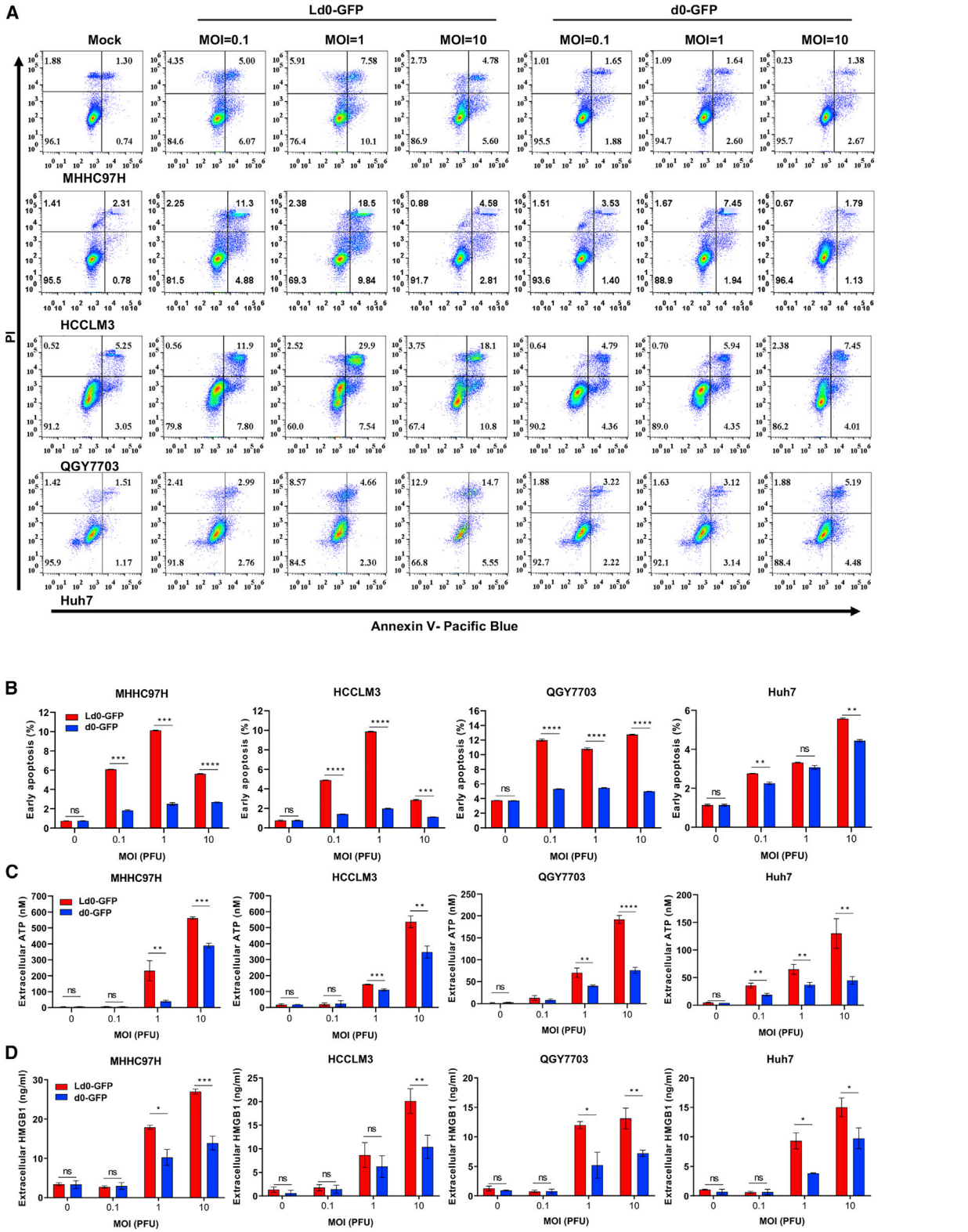

(legend on next page)

and orthotopic HCC model bearing mouse H22 HCC *in situ* (Figure 8A). For subcutaneous xenograft models, after the implanted tumor volume reached 100 mm^3, mice in each model were randomized to receive three doses of intratumoral injection of Ld0-GFP or d0-GFP (5×10^6 PFU per dose). Mice received PBS (vehicle) as a parallel negative control. It was observed that tumor growth was significantly inhibited in the Ld0-GFP-treated group compared to the d0-GFP-treated or vehicle-treated group (Figures 7B and 7D). The results showed that Ld0-GFP exhibited excellent therapeutic efficacy in HCC xenografted immunodeficient mice. Additionally, no obvious toxicity was observed in the virus-treated group during the treatment. However, obvious body weight change was observed in vehicle-treated groups, possibly due to the adverse effect of rapid tumor growth on nude mice (Figures 7C and 7E).

For the syngeneic HCC mouse model, after the implanted tumor volume reached 100 mm^3, mice were randomized to receive three doses of intravenous injection of Ld0-GFP or d0-GFP (1×10^7 PFU per dose). Mice received PBS (vehicle) as a parallel negative control. It was observed that tumor growth was significantly inhibited in the Ld0-GFP-treated group compared to the d0-GFP-treated or vehicle-treated group (Figure 8B), and prolonged survival time was observed in the Ld0-GFP-treated group (Figure 8C). Since mice from the vehicle-treated group started to die on day 30 after virus treatment, we thereafter followed up the long-term survival.

Ld0-GFP therapy induced robust tumor eradication and durable cures without relapse in 62.5% of the mice implanted with H22 tumors during a 150-day follow-up (Figure 8C), showing higher efficacy compared to d0-GFP therapy (durable cures in 37.5% of the mice). Moreover, we established orthotopic HCC mice bearing mouse H22 HCC *in situ* to evaluate the oncolytic efficacy of Ld0-GFP in the context of the liver microenvironment through three doses of intravenous injection of virus (1×10^7 PFU per dose); consistent with the previous subcutaneous xenograft models, remarkedly reduced tumor size and prolonged survival were observed in the Ld0-GFP-treated group (Figure 8D). As shown in Figure 8E, the liver tumor sizes were significantly reduced in the Ld0-GFP-treated group compared to the d0-GFP-treated at 10 or 20 days after the initial treatment.

DISCUSSION

Treatment options and their outcomes in HCC have not changed significantly in decades. Sorafenib has been the standard therapy for patients with unresectable HCC since 2007; however, the clinical efficacy of sorafenib is still unsatisfactory, and only 2–3 months of life was prolonged in patients with advanced HCC.[27] Lenvatinib has been demonstrated to be non-inferior to sorafenib in overall survival in untreated advanced HCC.[28] Recently, a combination therapy of lenvatinib and anti-PD-1 inhibitor has been suggested as a potential new treatment option for advanced HCC, but the potential toxicities of this form of immunotherapy are still largely unknown.[29] There is still an urgent need for improved, less toxic local agents for long-term HCC control. Therefore, the aim of this study was to investigate the potential of oncolytic Ld0-GFP as a new therapeutic agent against HCC.

Our study focused on developing a novel OV for HCC by enhancing the antitumor activities of an ICP0-null oncolytic HSV-1 (Ld0-GFP) in HCC cells. Of the 11 HCC cells tested, we found Ld0-GFP to be the most potent at killing in HCC cells. Surprisingly, the enhanced oncolysis is only restricted in HCC cells, but not in normal liver cell lines. Ld0-GFP showed a greater antitumor effect than d0-GFP but had less toxicities on normal cell lines. This agrees with published observations that show that the continuous adaptation of a virus in specific cell lines at a high MOI can result in a greater anti-cancer effect.[30,31] Due to the adaptation of Ld0-GFP in HCC cells, the majority of HCC cell lines studied were susceptible to direct oncolysis by Ld0-GFP. Ld0-GFP kills tumor cells efficiently and directly through both replication and cell membrane fusion. These two cytolytic mechanisms may also produce a synergistic effect through syncytial formation that facilitates the spread of the OV in tumor tissue as well as bystander killing of uninfected tumor cells.[32–34]

We sequenced the whole genomes of both d0-GFP and Ld0-GFP, and the amino acids of all open reading frames (ORFs) in the virus genome were compared (Table S1). Ld0-GFP had two vital syncytial mutations, gKsyn1 (Ala-to-Val at position 40) and gB (Glu-to-Asp at postion 816), which were reported to participate directly in the fusion of HSV-1-infected cells.[30,35–37] Other nonlethal mutations in the UL9, UL12, and UL13 genes were also observed, but not reported to participate directly in the fusion of HSV-1-infected cells, which may play a role in enhanced cell-killing ability of Ld0-GFP in HCC cells. Specifically, syncytial mutations that cause extensive virus-induced cell fusion can arise in at least two of the glycoproteins: glycoprotein K (gK) and glycoprotein B (gB).[30,37] Because the gB and gK are late genes of which the expressions are dependent on viral DNA replication, an OV carrying these syncytial mutations will maintain the safety of the original virus, because syncytial formation will only occur in replication-permissive tumor cells, but not in replication-restricted normal nondividing cells.[33] We hypothesized that Ld0-GFP may be modified on viral glycoproteins to increase the cell-killing ability

Figure 4. Ld0-GFP Can Induce Stronger Immunogenic Cell Death in HCC Cell Lines

(A) Determination of levels of early apoptosis in four HCC cell lines left uninfected or infected with Ld0-GFP or d0-GFP at MOIs of 0.1, 1, and 10 PFU/cell for 24 h by using annexin-V/PI-labeled flow cytometry. (B) Graphs represent pooled data from three independent experiments. (C) Determination of the level of ATP in the supernatants of four HCC cell lines left untreated or infected with Ld0-GFP or d0-GFP at MOIs of 0.1, 1, and 10 PFU/cell for 24 h. (D) Determination of the level of HMGB1 in the supernatants of four HCC cell lines left untreated or infected with Ld0-GFP or d0-GFP at MOIs of 0.1, 1, and 10 PFU/cell for 24 h. Graphs represent pooled data from three independent experiments. Values are the means of three independent experiments; data are shown as means ± SEM. Data were analyzed by unpaired two-tailed Student's t tests.

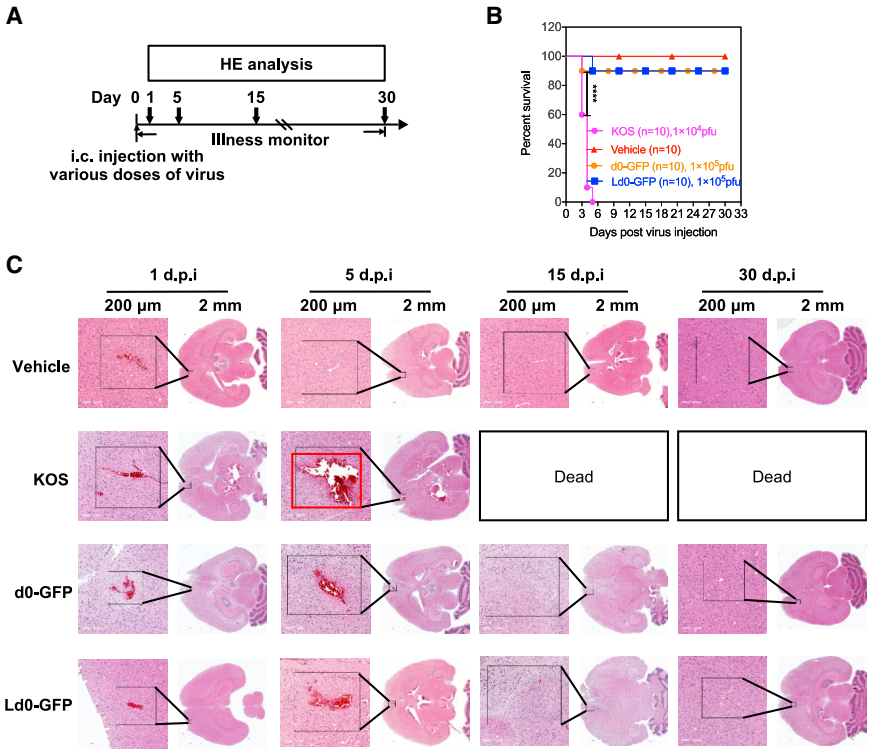

Figure 5. Neurovirulence Evaluation of Ld0-GFP in BALB/c Mice

(A) Treatment scheme. i.c., intracerebral. BALB/c mice were injected with KOS, d0-GFP, and Ld0-GFP viruses at the indicated dosage and followed for survival. (B) Survival analysis of BALB/c mice after treatment. (C) H&E staining of whole brains from vehicle-, KOS-, d0-GFP-, and Ld0-GFP-injected mice on day 1, 5, 15, and 30 following virus injection. Red box represents injured areas. Scale bars, 200 μm. Data for survival were analyzed by the log-rank (Mantel-Cox) test. All values are presented as the mean ± SEM. ****$p < 0.0001$.

in HCC cells, but not in normal hepatic cells, by introducing some syncytial mutations gK/A40V and gB/E816D, although the underlying mechanisms were not fully understood in this study.

In addition to the direct cytotoxic effect of OVs, it is also well recognized that the antitumor immunity of OVs may play a vital role in controlling tumor growth. It was reported that oncolytic adenovirus and herpes virus can induce the oncolysis of the cancer cells and make them release damage-associated molecular patterns (DAMPs) to induce innate immune response within the tumor, remodeling the tumor microenvironment from immunosuppressive to immune active.[38] Understanding the immunogenicity of dying or dead cancer cells induced by OVs is important when considering their potency for cancer immunotherapy.[39] Our study revealed that ICD was the primary death pattern induced by Ld0-GFP in HCC cells. Ld0-GFP possessed much higher capability to induce ICD than d0-GFP. To determine whether this Ld0-GFP-induced cell death was in fact immunogenic, the *in vitro* characteristics of ICD in HCC cells were investigated. Two type of DAMPs, released ATP and HMGB1, have been significantly induced after Ld0-GFP infection. Moreover, Ld0-GFP possessed much higher capability to release ICD determinants than d0-GFP. The importance of ICD for initiating an antitumor response has previously been demonstrated, so Ld0-GFP may have better potency to initiate an antitumor response by inducing ICD.[40]

In vivo, we demonstrated that virotherapy was more effective at promoting tumor regression in the subcutaneous xenograft model, syngeneic HCC mouse model, and orthotopic HCC model. As expected, intratumoral injection of Ld0-GFP exerted superior therapeutic effects on the HCC xenografts implanted on the nude mice and immunocompetent mice. We speculated that more active cell-killing capability of OV and enhanced immunogenic cell death may lead to better tumor regression. Although the correlation of oncolytic HSV replication/killing *in vitro* with antitumor activity in immunocompetent models has been challenged,[41,42] we believe that direct killing activity of OVs, magnitude of immunogenic cell death to release DAMPs, and initiation or augmentation of a host antitumor immune response should all play an essential role in oncolytic virotherapy. Moreover, intravenous injection of Ld0-GFP significantly prolonged the overall survival in the orthotopic HCC model, and the efficacy of Ld0-GFP systemic infusion is better than that of d0-GFP systemic infusion, thus demonstrating that Ld0-GFP may be amenable to systemic administration, thereby targeting metastatic disease. Overall, these data indicated that Ld0-GFP could be more effective as a single agent for both local and systemic treatments of HCC.[43]

A preliminary systemic toxicity assessment was conducted in BALB/c mice following intravenous injection of Ld0-GFP at a single high dose (5×10^7 PFU). Neither illness nor significant body weight loss was observed in the Ld0-GFP-treated and d0-GFP-treated groups, while the illness and significant body weight loss was observed in the KOS-treated group. Acute lung injury was found in KOS-injected mice, but not in Ld0-GFP-injected mice and d0-GFP-injected mice by histological analysis on days 1, 5, and 7 post-injection. Neurovirulence evaluation results showed that Ld0-GFP had similar neurovirulence similar to d0-GFP, both of them showing significantly lower neurovirulence than KOS. All these data demonstrate that Ld0-GFP possesses a safety profile with less toxicity and neurovirulence.[44]

Following the success of immune checkpoint inhibition in multiple solid tumors, there are numerous trials evaluating the role of anti-PD-1 agents in HCC.[45,46] Given the limited response rate (18%) in the management of advanced HCC, there is still an urgent need to create new strategies to maximize the potential of anti-PD-1

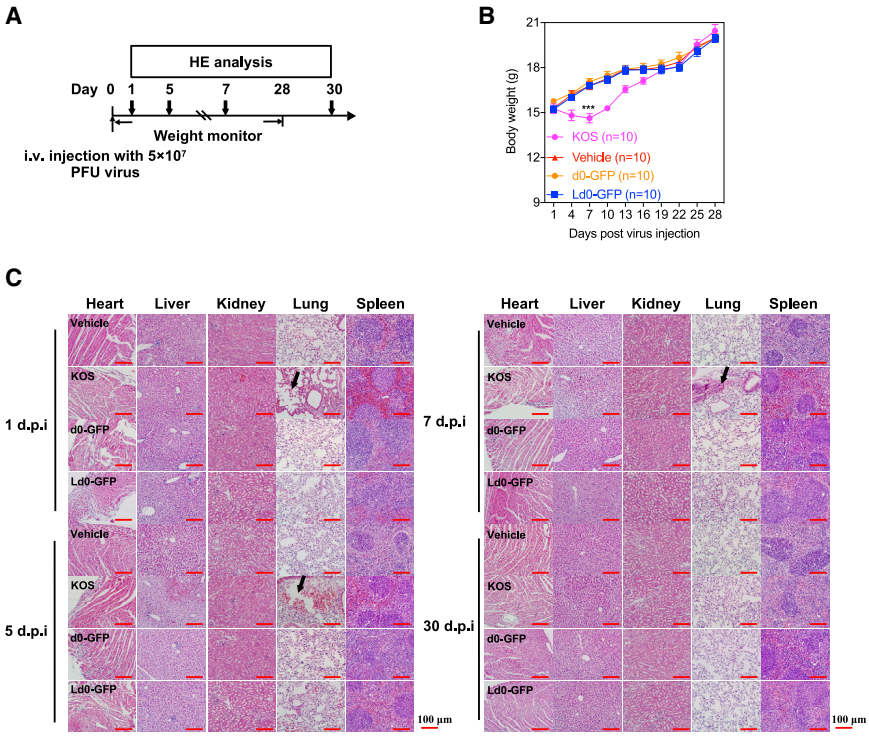

Figure 6. Systematic Toxicity Evaluation of Ld0-GFP in BALB/c Mice

(A) Treatment scheme. i.v., intravenous. BALB/c mice were injected with KOS, d0-GFP, and Ld0-GFP viruses at the indicated dosage and followed for survival. (B) Body weight monitoring of BALB/c mice after receiving a single dose of 5×10^7 PFU viruses through i.v. injection. Scale bars, 100 μm. (C) H&E staining of representative tissue sections from vehicle-, KOS-, d0-GFP-, and Ld0-GFP-injected mice on days 1, 5, 7, and 30 following virus injection. Black arrows represent lung injuries. The statistical significance of the intergroup comparisons of body weight was analyzed using a repeated-measure ANOVA. All values are presented as the mean ± SEM. ***$p < 0.001$.

immunotherapy. The development of OVs as novel immune sensitizers has recently accelerated; the most notable example is T-Vec, which helps overcome resistance to anti-PD-1 antibodies in patients with advanced melanoma, therefore promoting intratumoral T cell infiltration and improving anti-PD-1 immunotherapy. We are currently exploring the use of multiple sensitizers, including small molecular inhibitors and immune checkpoint antibodies,[47] to facilitate the effectiveness of Ld0-GFP.

In summary, this study developed a novel HSV-1 vector, Ld0-GFP, showing the increased tumor selectivity and improved oncolysis capability against HCC, which depends on efficient and selective viral replication and cancer cell killing in HCC cells. Furthermore, the utility of Ld0-GFP as a potent anti-cancer agent was demonstrated by its potential to elicit cell apoptosis and several ICD-related DAMPs. In addition, Ld0-GFP is efficacious in three preclinical tumor models by systemic infusion or intratumoral injection, and it is relatively safe for the mice treated by systemic infusion or intracerebral injection. The findings from this study have provided the rationale for the application of a novel OV in treating HCC. The antitumor potential of Ld0-GFP may be potentially enhanced by sequential administration or co-administration of other agents to increase virus spread and replication, as well as in combination with immune checkpoint inhibitors.[48]

MATERIALS AND METHODS

Cells

Huh7, SMMC7721, QGY7703, L-02, BEL7404, GSG7701, HCCLM3, MHHC97H, H22, and HCT116 were purchased from the China Infrastructure of Cell Line Resources (Beijing, China). HepG2, Hep3B, U-2 OS, SK-HEP-1, PLC/PRF/5, and H1299 were purchased from the American Type Culture Collection (Manassas, VA, USA). U-2 OS, Huh7, HepG2, Hep3B, SK-HEP-1, PLC/PRF/5, HCT116, and H1299 were cultured in DMEM supplemented with 10% (v/v) fetal bovine serum (FBS) (Invitrogen, CA, USA). SMMC7721, L-02, BEL7404, QGY7703, GSG7701, HCCLM3, MHHC97H, and H22 were cultured in 1640 supplemented with 10% (v/v) FBS (Invitrogen, CA, USA). All cells were maintained at 37°C and 5% CO_2.

Viruses and Virus Generation

Ld0-GFP used in this study is based on the d0-GFP virus, which was generated as described previously in our laboratory.[24] The d0-GFP virus was bearing the EGFP reporter genes under the control of the human cytomegalovirus promoter replacing the viral ICP0 genes. Ld0-GFP was produced by continuous passage of d0-GFP in three HCC cells (Hep3B, QGY7703, and SMMC7721) until the fusogenic plaques were observed. For every round of d0-GFP passage, these three HCC cancer cell lines were sequentially infected with viruses at an MOI of 1 and then harvested at 72 h post-infection for subsequent re-infection. Each HCC cell line was infected at least twice. After seven rounds of repeated infection, the harvested viruses were subjected to two rounds of freeze and thaw cycles and serially diluted for infection of U-2 OS monolayers. After three passages of plaque purification in cell culture, the EGFP reporter genes and plaques with fusogenic feature were used to select and isolate the random mutant viruses.

Ten fusogenic d0-GFP progenies were picked out and evaluated by testing the replication difference and cell-killing percentages on both HCC cell lines (QGY7703) and the hepatic normal cell line (L-02). For the replication efficiency assay, the U-2 OS cells were infected with d0-GFP or d0-GFP progenies at an MOI of 0.05 PFU. After 72 h of infection, the infected cells together with the supernatants were collected and thereafter subjected to virus titration. For

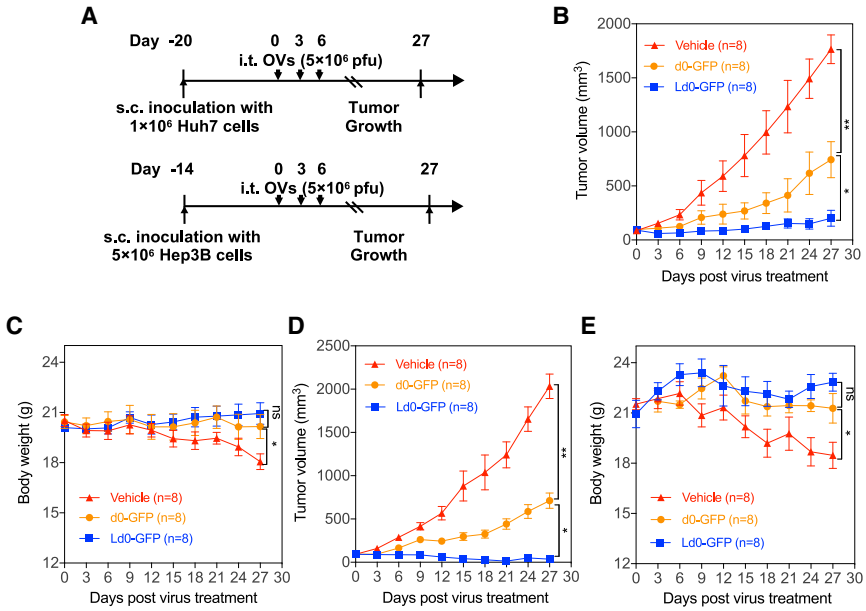

Figure 7. Oncolytic Efficacy of Ld0-GFP in the Subcutaneous Xenograft Model Bearing Human HCC

(A) Treatment scheme. s.c., subcutaneous. (B) Growth of vehicle-, d0-GFP- or Ld0-GFP-treated Huh7 xenografts in nude mice (n = 8). (C) Body weight of the treated nude mice was monitored in the subcutaneous Huh7 xenograft model. (D) Growth of vehicle-, d0-GFP- or Ld0-GFP-treated Hep3B xenografts in nude mice (n = 8). (E) Body weight of the treated nude mice was monitored in the subcutaneous Hep3B xenograft model. The statistical significance of the intergroup comparisons of tumor volumes or body weight was analyzed using a repeated-measure ANOVA. All values are presented as the mean ± SEM. *p < 0.05, **p < 0.01, ns, not significant.

the cell-killing ability assay, cells were infected with d0-GFP or d0-GFP progenies at an MOI of 0.001–10 PFU/cell. After 72 h of infection, the number of viable cells was counted by the trypan blue exclusion method. Finally, a novel virus (d0-GFP-7, named Ld0-GFP) with relatively higher replication efficiency in U-2 OS and the highest cell-killing activity in HCC cells (QGY7703), but not in liver normal cells (L-02), was obtained. The IC_{50} was interpreted and calculated by non-linear, dose-response regression analysis.

Virus Titration

The titers of the amplified viruses were determined on U-2 OS monolayers using a classical plaque assay. In brief, a monolayer of U-2 OS cells at a density of 2×10^6 cells per 6-cm dish was infected with serially diluted virus in a volume of 0.5 mL for 1.25 h. After viral entry, the cells were overlaid with 2% methylcellulose medium and incubated at 37°C in 5% CO_2 for 2 days. Then, the dishes were stained with neutral red overnight, and the plaques were counted manually using a white-light transilluminator (Qilinbeier, China). Viral titers (PFU/mL) were calculated using the equation plaque numbers × dilution fold × 2.

Virus Replication Assay

Cells were seeded in 6-cm plates at 10^6 cells/dish and infected with Ld0-GFP (0.05 PFU/cell) or mock infected (10% DMEM). For each time point, the infected cells were either harvested and thereafter subjected to virus titration or examined by fluorescence microscopy.

Evaluation of the Size of Virus Plaques

To determine the plaque size from the various viruses assayed, SMMC7721 monolayers were infected with diluted d0-GFP and Ld0-GFP viruses in 2% methylcellulose medium. After 48 h of infection, the dishes were stained with medium containing 0.01% neutral red overnight, and the visualized virus plaques were photographed. The size of the plaques was measured with a millimeter scale using ImageJ software, and the area for comparison was calculated using the following formula: area = (π) × (radius of the minor axis) × (radius of the largest axis).

Cell-Killing Assay

Cells were seeded in 6-well plates at 1×10^6 cells/well and infected with d0-GFP or Ld0-GFP at various MOIs of 0.001–10 PFU. For each time point, cell viability was expressed as the percentage of viable cells, which were counted by the trypan blue exclusion method. The IC_{50} values were interpreted and calculated as previously described.

Cell Death Assay

Cells were infected with d0-GFP or Ld0-GFP at MOIs of 0.1, 1, and 10 PFU/cell or with mock (10% DMEM). After 24 h of infection, the cells were harvested and stained with annexin V, Pacific Blue flow cytometry kit (Invitrogen, CA, USA) and PI. Apoptotic cell death was determined by FACS analysis using the BD FACSDiva Software on a FACSAria II cell sorter (Becton Dickinson, NJ, USA). ELISA analysis was used to determine the expression of ICD determinants in the supernatants of treated cells. Cells were infected with d0-GFP or Ld0-GFP at MOIs of 0.1, 1, and 10 PFU/cell and mock (10% DMEM). After 24 h of infection, the supernatants were harvested. The released ATP was measured by an ATPlite Luminescence kit (PerkinElmer, MA, USA), and the HMGB1 was measured by an HMGB1 ELISA kit (Tecan, Switzerland).

Animal Experiments

The use of the mice was approved by the Institutional Animal Care and Use Committee at Xiamen University (XMULAC20150016). All mice were purchased from Shanghai Slack Laboratory Animal, and they were housed under specific-pathogen-free conditions in a chamber with controlled temperature and humidity.

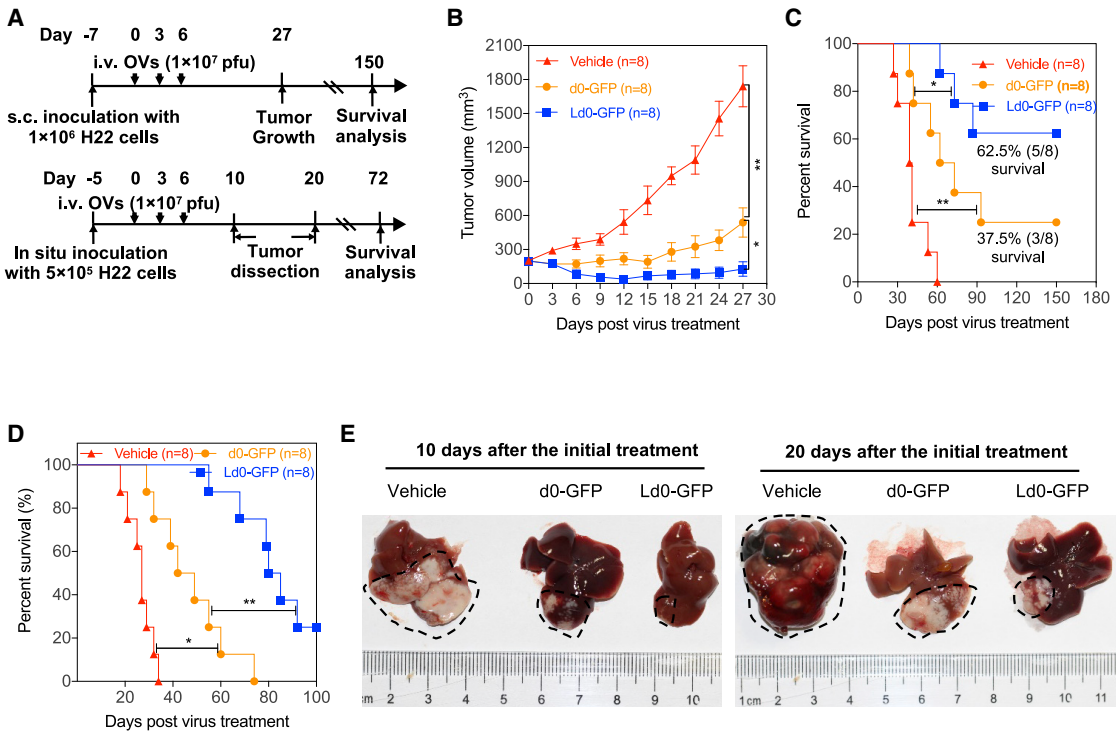

Figure 8. Oncolytic Efficacy of Ld0-GFP in Syngeneic HCC Mouse Models

(A) Treatment scheme. i.v., intravenous. (B) Growth of vehicle-, d0-GFP-, or Ld0-GFP-treated H22 tumors in immunocompetent BALB/c mice (n = 8). (C) Long-term survival of BALB/c mice bearing H22 tumors. (D) Long-term survival in orthotopic HCC model bearing mouse H22 HCC *in situ*, after receiving three i.v. treatments of Ld0-GFP (1×10^7 PFU) or vehicle (n = 8). (E) Representative images of livers from each group on days 10 and 20 following virus i.v. injection. Dashed black lines represent tumor areas. The statistical significance of the intergroup comparisons of tumor volumes or body weight was analyzed using a repeated-measure ANOVA. Data for survival were analyzed by the log-rank (Mantel-Cox) test. All values are presented as the mean ± SEM. *$p < 0.05$, **$p < 0.01$; ns, not significant.

Subcutaneous Xenograft Model

An inoculum of 1×10^6 Huh7 or 5×10^6 Hep3B cells was injected subcutaneously into the flank of 5-week-old female BALB/c nu/nu mice in 50 μL sterile PBS. After 20 or 14 days, Huh7 tumors or Hep3B tumors reached an average size of ~100 mm^3. Mice were randomized into treatment groups immediately prior to treatment. Virus (5×10^6 PFU) or vehicle (saline) was administered via intratumoral injection every 3 days for three consecutive dosages in total. Tumor growth and body weight were monitored every 3 days. At 21 days after the last treatment, mice received their final measurements, and the volume was calculated according to the following formula: (length × $width^2$)/2.

Syngeneic HCC Model

An inoculum of 10^6 murine HCC cells (H22) was injected subcutaneously into the flank of 6-week-old female BALB/c mice in 50 μL sterile PBS. Mice were randomized into treatment groups on day 7 following tumor inoculation, immediately before treatment. Virus (1×10^7 PFU) or vehicle (saline) was administered via intravenous injection every 3 days for three consecutive dosages in total. Tumor growth and body weight were monitored every 3 days, and the volume was calculated according to the following formula: (length × $width^2$)/2. The overall survival of mice was monitored over a 150-day period.

Orthotopic HCC Model

An inoculum of 5×10^5 murine HCC cells (H22) was implanted into the left liver lobe of 6-week-old female BALB/c mice in 20 μL sterile PBS. After 5 days, the mice were randomized into treatment groups immediately before treatment. Virus (1×10^7 PFU) or vehicle (saline) was administered by tail vein injection every 3 days for three consecutive dosages in total. The overall survival of mice was monitored over a 100-day period. Representative images of livers in Ld0-GFP- and d0-GFP-treated mice were taken 10 and 20 days after the initial treatment.

Neurovirulence Study

The 5-week-old female BALB/c mice were randomly assigned to four groups of 18 mice each; mice were anesthetized with sodium thiopental (60 mg/kg) and inoculated with vehicle (saline), KOS, d0-GFP, and Ld0-GFP by intracerebral injection into the left frontal lobe of the brain, in a volume of 5 μL at a depth of 4.5 mm from the skull surface over a period of 10 min. Ten mice of each group

were monitored for signs and symptoms of illness for 30 days following inoculation. For each time point (at 1, 5, 15, and 30 days post-injection), two mice of each group were examined for histology analysis. Paraffin sections (5 μm thick) of brain of BALB/c mice were stained with H&E.

Systemic Toxicity Study

The 6-week-old female BALB/c mice were randomly assigned to four groups of 18 mice each; mice were inoculated with vehicle (saline), KOS, d0-GFP, and Ld0-GFP by intravenous injection into the tail vein at a dose of 5×10^7 PFU in a volume of 500 μL over a period of 2 min. Ten mice of each group were monitored for weights and examined for histology analysis at 1, 5, 7, and 30 days post-injection. Paraffin sections (5 μm thick) of vital tissues (including heart, liver, spleen, lung, and kidney) of BALB/c mice (two mice for each group) were stained with H&E.

Genome Sequencing

d0-GFP and Ld0-GFP genomic DNA were isolated from infected U-2 OS cells using standard protocols.[49] An unpaired 350-bp Illumina library was generated and double-end sequenced using the HiSeq sequencing platform (Novogene). The resulting reads were assembled initially into large contigs. All ORFs in the virus genome were compared between d0-GFP and Ld0-GFP, using KOS genome sequence (GenBank: JQ673480) as a reference.

Statistics

Statistical significance was calculated using the unpaired two-tailed Student's t test (if the values follow normal distribution) or a repeated-measure ANOVA, as indicated in the figure legends. Data for survival was analyzed by the log-rank (Mantel-Cox) test. For all statistical analyses, differences were considered significant when a p value was below or equal to 0.05 (*$p < 0.05$, **$p < 0.01$, ***$p < 0.001$, and ****$p < 0.0001$; ns, not significant). Statistical analyses were performed using GraphPad Prism 7. The numbers of animals included in the study are labeled in each figure.

SUPPLEMENTAL INFORMATION

Supplemental Information can be found online at https://doi.org/10.1016/j.omto.2019.09.004.

AUTHOR CONTRIBUTIONS

Y.L., C.L., W.R., F.J., Z.X., H.L., Z.Y., and J.C. conducted the experiments. C.H. and J.Z. interpreted the data. C.H., N.X., and P.L. designed the experiments and wrote the paper.

CONFLICTS OF INTEREST

The authors declare no competing interests.

ACKNOWLEDGMENTS

This work was supported by the National Science and Technology Major Project of China (grants 2018ZX10301404-001-002 and 2018) and the National Natural Science Foundation of China (grant 81571990).

REFERENCES

1. Fitzmaurice, C., Akinyemiju, T.F., Al Lami, F.H., Alam, T., Alizadeh-Navaei, R., Allen, C., Alsharif, U., Alvis-Guzman, N., Amini, E., Anderson, B.O., et al.; Global Burden of Disease Cancer Collaboration (2018). Global, Regional, and National Cancer Incidence, Mortality, Years of Life Lost, Years Lived With Disability, and Disability-Adjusted Life-Years for 29 Cancer Groups, 1990 to 2016: A Systematic Analysis for the Global Burden of Disease Study. JAMA Oncol. *4*, 1553–1568.
2. Siegel, R., Naishadham, D., and Jemal, A. (2013). Cancer statistics, 2013. CA Cancer J. Clin. *63*, 11–30.
3. El-Serag, H.B. (2011). Hepatocellular carcinoma. N. Engl. J. Med. *365*, 1118–1127.
4. Balogh, J., Victor, D., 3rd, Asham, E.H., Burroughs, S.G., Boktour, M., Saharia, A., Li, X., Ghobrial, R.M., and Monsour, H.P., Jr. (2016). Hepatocellular carcinoma: a review. J. Hepatocell. Carcinoma *3*, 41–53.
5. Russell, S.J., Peng, K.W., and Bell, J.C. (2012). Oncolytic virotherapy. Nat. Biotechnol. *30*, 658–670.
6. Kaufman, H.L., Kohlhapp, F.J., and Zloza, A. (2015). Oncolytic viruses: a new class of immunotherapy drugs. Nat. Rev. Drug Discov. *14*, 642–662.
7. Heo, J., Reid, T., Ruo, L., Breitbach, C.J., Rose, S., Bloomston, M., Cho, M., Lim, H.Y., Chung, H.C., Kim, C.W., et al. (2013). Randomized dose-finding clinical trial of oncolytic immunotherapeutic vaccinia JX-594 in liver cancer. Nat. Med. *19*, 329–336.
8. Killock, D. (2015). Skin cancer: T-VEC oncolytic viral therapy shows promise in melanoma. Nat. Rev. Clin. Oncol. *12*, 438.
9. Lawler, S.E., Speranza, M.C., Cho, C.F., and Chiocca, E.A. (2017). Oncolytic Viruses in Cancer Treatment: A Review. JAMA Oncol. *3*, 841–849.
10. Ribas, A., Dummer, R., Puzanov, I., VanderWalde, A., Andtbacka, R.H.I., Michielin, O., Olszanski, A.J., Malvehy, J., Cebon, J., Fernandez, E., et al. (2018). Oncolytic Virotherapy Promotes Intratumoral T Cell Infiltration and Improves Anti-PD-1 Immunotherapy. Cell *174*, 1031–1032.
11. Sanchala, D.S., Bhatt, L.K., and Prabhavalkar, K.S. (2017). Oncolytic Herpes Simplex Viral Therapy: A Stride toward Selective Targeting of Cancer Cells. Front. Pharmacol. *8*, 270.
12. Zhang, S.X. (2015). Turning killer into cure – the story of oncolytic herpes simplex viruses. Discov. Med. *20*, 303–309.
13. Bommareddy, P.K., Peters, C., Saha, D., Rabkin, S.D., and Kaufman, H.L. (2018). Oncolytic Herpes Simplex Viruses as a Paradigm for the Treatment of Cancer. Annu. Rev. Cancer Biol. *2*, 155–173.
14. Nakatake, R., Kaibori, M., Nakamura, Y., Tanaka, Y., Matushima, H., Okumura, T., Murakami, T., Ino, Y., Todo, T., and Kon, M. (2018). Third-generation oncolytic herpes simplex virus inhibits the growth of liver tumors in mice. Cancer Sci. *109*, 600–610.
15. Abdullahi, S., Jäkel, M., Behrend, S.J., Steiger, K., Topping, G., Krabbe, T., Colombo, A., Sandig, V., Schiergens, T.S., Thasler, W.E., et al. (2018). A Novel Chimeric Oncolytic Virus Vector for Improved Safety and Efficacy as a Platform for the Treatment of Hepatocellular Carcinoma. J. Virol. *92*, e01386-18.
16. Argnani, R., Marconi, P., Volpi, I., Bolanos, E., Carro, E., Ried, C., Santamaria, E., Pourchet, A., Epstein, A.L., Brocker, T., et al. (2011). Characterization of herpes simplex virus 1 strains as platforms for the development of oncolytic viruses against liver cancer. Liver Int. *31*, 1542–1553.
17. Fu, X., Tao, L., Jin, A., Vile, R., Brenner, M.K., and Zhang, X. (2003). Expression of a fusogenic membrane glycoprotein by an oncolytic herpes simplex virus potentiates the viral antitumor effect. Mol. Ther. *7*, 748–754.
18. Jarnagin, W.R., Zager, J.S., Klimstra, D., Delman, K.A., Malhotra, S., Ebright, M., Little, S., DeRubertis, B., Stanziale, S.F., Hezel, M., et al. (2003). Neoadjuvant treatment of hepatic malignancy: an oncolytic herpes simplex virus expressing IL-12 effectively treats the parent tumor and protects against recurrence-after resection. Cancer Gene Ther. *10*, 215–223.
19. Miao, L., Fraefel, C., Sia, K.C., Newman, J.P., Mohamed-Bashir, S.A., Ng, W.H., and Lam, P.Y. (2014). The potential application of a transcriptionally regulated oncolytic herpes simplex virus for human cancer therapy. Br. J. Cancer *110*, 94–106.
20. Foka, P., Pourchet, A., Hernandez-Alcoceba, R., Doumba, P.P., Pissas, G., Kouvatsis, V., Dalagiorgou, G., Kazazi, D., Marconi, P., Foschini, M., et al. (2010). Novel

tumour-specific promoters for transcriptional targeting of hepatocellular carcinoma by herpes simplex virus vectors. J. Gene Med. *12*, 956–967.

21. Miyatake, S.I., Tani, S., Feigenbaum, F., Sundaresan, P., Toda, H., Narumi, O., Kikuchi, H., Hashimoto, N., Hangai, M., Martuza, R.L., and Rabkin, S.D. (1999). Hepatoma-specific antitumor activity of an albumin enhancer/promoter regulated herpes simplex virus in vivo. Gene Ther. *6*, 564–572.
22. Fu, X., Rivera, A., Tao, L., De Geest, B., and Zhang, X. (2012). Construction of an oncolytic herpes simplex virus that precisely targets hepatocellular carcinoma cells. Mol. Ther. *20*, 339–346.
23. Jebar, A.H., Errington-Mais, F., Vile, R.G., Selby, P.J., Melcher, A.A., and Griffin, S. (2015). Progress in clinical oncolytic virus-based therapy for hepatocellular carcinoma. J. Gen. Virol. *96*, 1533–1550.
24. Lin, C., Li, H., Hao, M., Xiong, D., Luo, Y., Huang, C., Yuan, Q., Zhang, J., and Xia, N. (2016). Increasing the Efficiency of CRISPR/Cas9-mediated Precise Genome Editing of HSV-1 Virus in Human Cells. Sci. Rep. *6*, 34531.
25. Hummel, J.L., Safroneeva, E., and Mossman, K.L. (2005). The role of ICP0-Null HSV-1 and interferon signaling defects in the effective treatment of breast adenocarcinoma. Mol. Ther. *12*, 1101–1110.
26. Galluzzi, L., Buqué, A., Kepp, O., Zitvogel, L., and Kroemer, G. (2017). Immunogenic cell death in cancer and infectious disease. Nat. Rev. Immunol. *17*, 97–111.
27. Llovet, J.M., Ricci, S., Mazzaferro, V., Hilgard, P., Gane, E., Blanc, J.F., de Oliveira, A.C., Santoro, A., Raoul, J.L., Forner, A., et al.; SHARP Investigators Study Group (2008). Sorafenib in advanced hepatocellular carcinoma. N. Engl. J. Med. *359*, 378–390.
28. Kudo, M., Finn, R.S., Qin, S., Han, K.H., Ikeda, K., Piscaglia, F., Baron, A., Park, J.W., Han, G., Jassem, J., et al. (2018). Lenvatinib versus sorafenib in first-line treatment of patients with unresectable hepatocellular carcinoma: a randomised phase 3 non-inferiority trial. Lancet *391*, 1163–1173.
29. Kudo, M. (2017). Lenvatinib in Advanced Hepatocellular Carcinoma. Liver Cancer *6*, 253–263.
30. Israyelyan, A., Chouljenko, V.N., Baghian, A., David, A.T., Kearney, M.T., and Kousoulas, K.G. (2008). Herpes simplex virus type-1(HSV-1) oncolytic and highly fusogenic mutants carrying the NV1020 genomic deletion effectively inhibit primary and metastatic tumors in mice. Virol. J. *5*, 68.
31. Howells, A., Marelli, G., Lemoine, N.R., and Wang, Y. (2017). Oncolytic Viruses-Interaction of Virus and Tumor Cells in the Battle to Eliminate Cancer. Front. Oncol. *7*, 195.
32. Ahmed, A., Jevremovic, D., Suzuki, K., Kottke, T., Thompson, J., Emery, S., Harrington, K., Bateman, A., and Vile, R. (2003). Intratumoral expression of a fusogenic membrane glycoprotein enhances the efficacy of replicating adenovirus therapy. Gene Ther. *10*, 1663–1671.
33. Fu, X., and Zhang, X. (2002). Potent systemic antitumor activity from an oncolytic herpes simplex virus of syncytial phenotype. Cancer Res. *62*, 2306–2312.
34. Nakamori, M., Fu, X., Meng, F., Jin, A., Tao, L., Bast, R.C., Jr., and Zhang, X. (2003). Effective therapy of metastatic ovarian cancer with an oncolytic herpes simplex virus incorporating two membrane fusion mechanisms. Clin. Cancer Res. *9*, 2727–2733.
35. Person, S., Kousoulas, K.G., Knowles, R.W., Read, G.S., Holland, T.C., Keller, P.M., and Warner, S.C. (1982). Glycoprotein processing in mutants of HSV-1 that induce cell fusion. Virology *117*, 293–306.
36. Bzik, D.J., Fox, B.A., DeLuca, N.A., and Person, S. (1984). Nucleotide sequence of a region of the herpes simplex virus type 1 gB glycoprotein gene: mutations affecting rate of virus entry and cell fusion. Virology *137*, 185–190.
37. Avitabile, E., Lombardi, G., and Campadelli-Fiume, G. (2003). Herpes simplex virus glycoprotein K, but not its syncytial allele, inhibits cell-cell fusion mediated by the four fusogenic glycoproteins, gD, gB, gH, and gL. J. Virol. *77*, 6836–6844.
38. Jiang, H., and Fueyo, J. (2014). Healing after death: antitumor immunity induced by oncolytic adenoviral therapy. OncoImmunology *3*, e947872.
39. Workenhe, S.T., and Mossman, K.L. (2014). Oncolytic virotherapy and immunogenic cancer cell death: sharpening the sword for improved cancer treatment strategies. Mol. Ther. *22*, 251–256.
40. van Vloten, J.P., Workenhe, S.T., Wootton, S.K., Mossman, K.L., and Bridle, B.W. (2018). Critical Interactions between Immunogenic Cancer Cell Death, Oncolytic Viruses, and the Immune System Define the Rational Design of Combination Immunotherapies. J. Immunol. *200*, 450–458.
41. Davola, M.E., and Mossman, K.L. (2019). Oncolytic viruses: how "lytic" must they be for therapeutic efficacy? OncoImmunology *8*, e1581528.
42. Workenhe, S.T., Simmons, G., Pol, J.G., Lichty, B.D., Halford, W.P., and Mossman, K.L. (2014). Immunogenic HSV-mediated oncolysis shapes the antitumor immune response and contributes to therapeutic efficacy. Mol. Ther. *22*, 123–131.
43. Ferguson, M.S., Lemoine, N.R., and Wang, Y. (2012). Systemic delivery of oncolytic viruses: hopes and hurdles. Adv. Virol. *2012*, 805629.
44. Fountzilas, C., Patel, S., and Mahalingam, D. (2017). Review: Oncolytic virotherapy, updates and future directions. Oncotarget *8*, 102617–102639.
45. Iñarrairaegui, M., Melero, I., and Sangro, B. (2018). Immunotherapy of Hepatocellular Carcinoma: Facts and Hopes. Clin. Cancer Res. *24*, 1518–1524.
46. Kudo, M. (2017). Immune Checkpoint Inhibition in Hepatocellular Carcinoma: Basics and Ongoing Clinical Trials. Oncology *92* (*Suppl 1*), 50–62.
47. Kohlhapp, F.J., and Kaufman, H.L. (2016). Molecular Pathways: Mechanism of Action for Talimogene Laherparepvec, a New Oncolytic Virus Immunotherapy. Clin. Cancer Res. *22*, 1048–1054.
48. Jhawar, S.R., Thandoni, A., Bommareddy, P.K., Hassan, S., Kohlhapp, F.J., Goyal, S., Schenkel, J.M., Silk, A.W., and Zloza, A. (2017). Oncolytic Viruses-Natural and Genetically Engineered Cancer Immunotherapies. Front. Oncol. *7*, 202.
49. Maclean, A.R. (1998). Preparation of HSV-DNA and Production of Infectious Virus. Methods Mol. Med. *10*, 19–25.

OMTO, Volume *15*

Supplemental Information

Intravenous Injections of a Rationally Selected Oncolytic Herpes Virus as a Potent Virotherapy for Hepatocellular Carcinoma

Yong Luo, Chaolong Lin, Wenfeng Ren, Fei Ju, Zilong Xu, Huiling Liu, Zeng Yu, Jun Chen, Jun Zhang, Pingguo Liu, Chenghao Huang, and Ningshao Xia

Figure S1

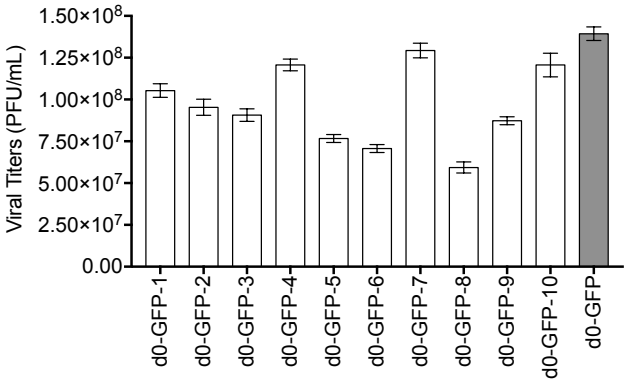

Figure S1. Assessing viral replication efficiency of fusogenic d0-GFP progenies. Viral titer was measured in various infected U-2 OS cell lines at 72 h after virus infection.

Figure S2

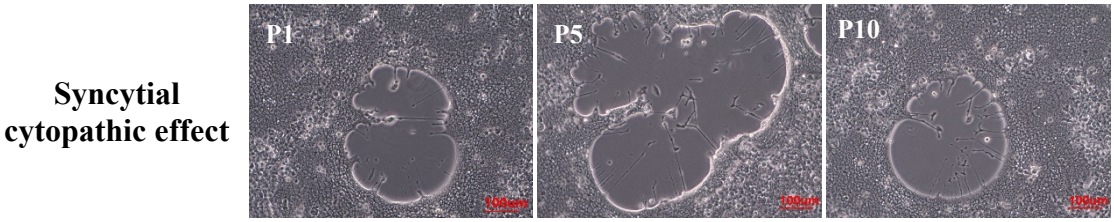

Figure S2. Syncytial cytopathic effect of Ld0-GFP progenies. Observation of Ld0-GFP plaque patterns were monitored at 48 h after virus infection (MOI=0.1 PFU/cell). P1 represents one time of passage, P5 represents five times of passage, P10 represents ten times of passage.

Figure S3

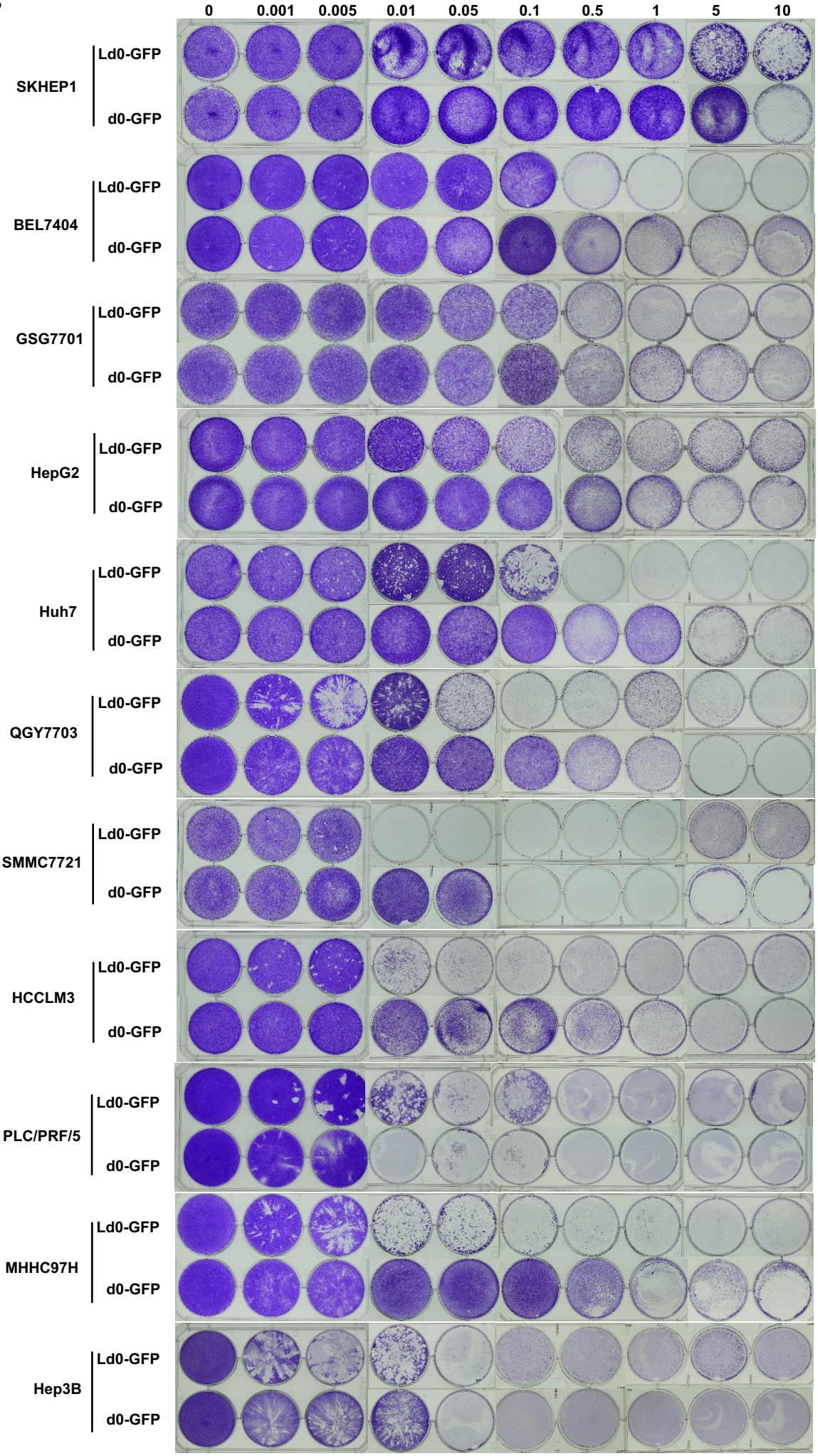
0
0.001
0.005
0.01
0.05
0.1
0.5
1
5
10
SKHEP1
Ld0-GFP
d0-GFP
BEL7404
Ld0-GFP
d0-GFP
GSG7701
Ld0-GFP
d0-GFP
HepG2
Ld0-GFP
d0-GFP
Huh7
Ld0-GFP
d0-GFP
QGY7703
Ld0-GFP
d0-GFP
SMMC7721
Ld0-GFP
d0-GFP
HCCLM3
Ld0-GFP
d0-GFP
PLC/PRF/5
Ld0-GFP
d0-GFP
MHHC97H
Ld0-GFP
d0-GFP
Hep3B
Ld0-GFP
d0-GFP

Figure S3. Oncolytic ability of Ld0-GFP and d0-GFP against different HCC cell lines. Cell viability assays were performed on a panel of HCC cell lines on 72 h post Ld0-GFP or d0-GFP infection (MOI=0.001~10 PFU/cell), respectively. Crystal violet staining was used to determine the remaining HCC cells after oncolysis.

Figure S4

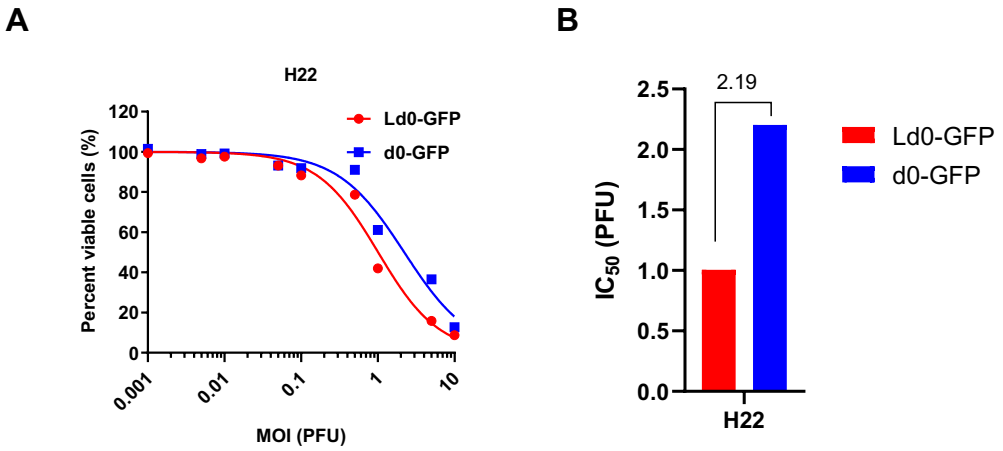

Figure S4. Oncolytic ability of Ld0-GFP and d0-GFP against murine H22 cell lines. (A) Cell viability assays were performed on murine H22 cell lines on 72 h post Ld0-GFP or d0-GFP infection (MOI=0.001~10 PFU/cell). (B) IC50 was calculated in various infected murine H22 cell lines.

Figure S5

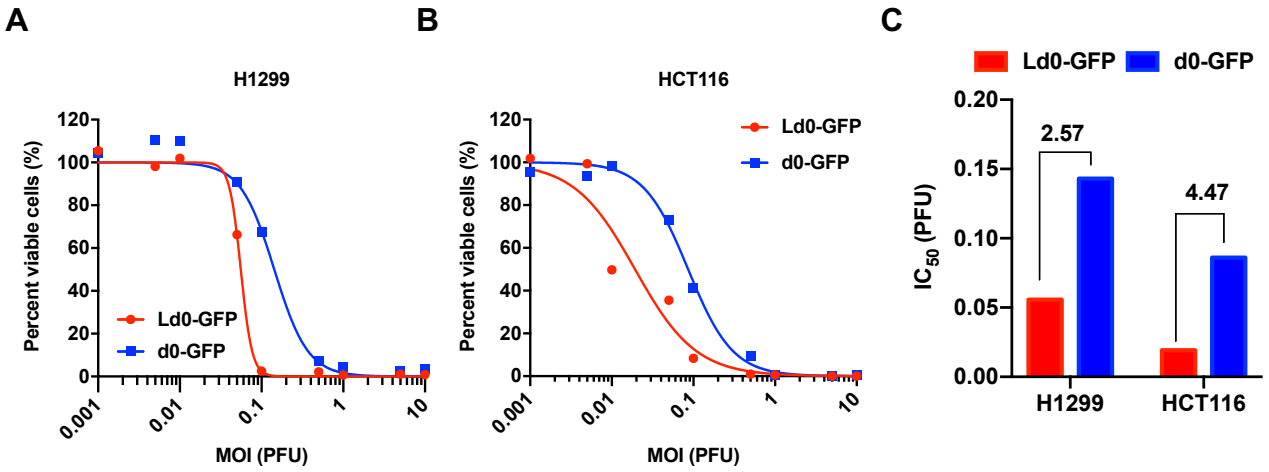

Figure S5. Oncolytic ability of Ld0-GFP and d0-GFP against non-HCC cell lines. (A) Cell viability assays were performed on the HCT116 and H1299 cell lines on 72 h post Ld0-GFP or d0-GFP infection (MOI=0.001~10 PFU/cell), respectively. (B) IC50 was calculated in various infected cancer cell lines.

Figure S6

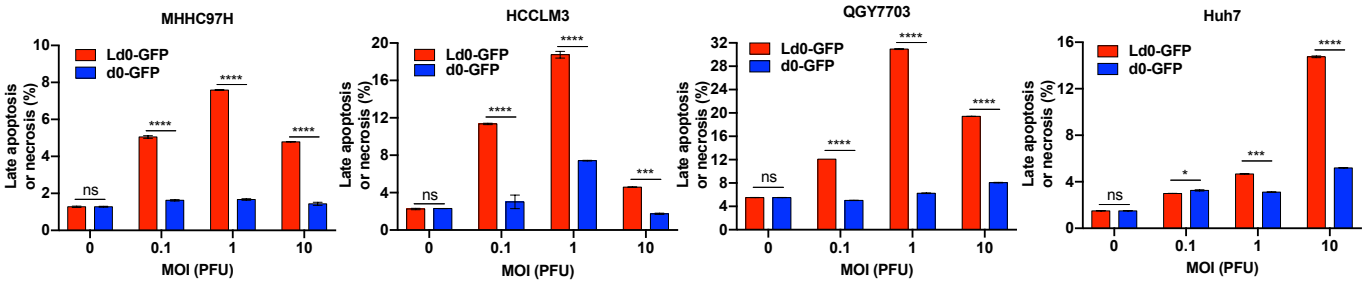

Figure S6. Ld0-GFP can induce stronger late apoptosis or necrosis in HCC cell lines. (A) Determination of levels of late apoptosis or necrosis in four HCC cell lines left uninfected or infected with Ld0-GFP or d0-GFP at MOIs of 0.1, 1 and 10 PFU/cell for 24 h by using annexin-V/PI-labeled flow cytometry.

Table S1. Amino acid sequence variation of Ld0-GFP relative to d0-GFP

ORF	Protein name	Function of gene product	Amino acid substitution	Possible impact of amino acid substitution on virus phenotype
UL9	UL9	Helicases; Required for HSV-1 DNA replication	A797P	Unknown
UL12	NUC	Alkaline nuclease; essential for viral replication.	A467T	Unknown
UL13	VPK	Virion (nuclear) protein kinase; substrates include ICP0, ICP22, etc.	D376E	Unknown
UL27	gB	Associate with membrane fusion.	E816D	Causes extensive virus-induced cell fusion.
UL53	gK	Glycoprotein required for efficient viral exocytosis; contains Syncytial-locus.	A40V	Display a reduced ability to block cell-cell fusion and endow fusogenicity.

The amino acids of all ORF in the virus genome were compared between d0-GFP and Ld0-GFP. Five genes, including UL53 (gK), UL27 (gB), UL9, UL12 (NUC) and UL13 (VPK), had amino acid changes unique to Ld0-GFP.